Comparison of high-fidelity aero-structure gradient computation techniques. Application on the CRM wing design

Timothée Achard, Christophe Blondeau, Roger Ohayon

COMPARISON OF HIGH-FIDELITY AERO-STRUCTURE GRADIENT COMPUTATION TECHNIQUES. APPLICATION ON THE CRM WING DESIGN.

Timothée Achard[1], **Christophe Blondeau**[1], **Roger Ohayon**[2]

[1]ONERA - The French Aerospace Lab, F-92322 Châtillon, France
Aerodynamics, Aeroelasticity and Aeroacoustics Department
timothee.achard@onera.fr,christophe.blondeau@onera.fr

[2]CNAM - 2 rue Conté, F-75003 Paris, France

Keywords: Sensitivity analysis, Multidisciplinary Optimization, Adjoint method

Abstract: Aero-structural optimization is a keystone to concurrently improve aerodynamic performance and reduce the structural mass of an aircraft. Gradient-based multi-disciplinary design optimization is actually efficient if gradients computations are fast and accurate enough. This paper presents two high-fidelity aero-structure gradient computation techniques for design variables impacting the stiffness of the structure. A first part details the new module developed and implemented in the Onera ***elsA*** software capable of computing aero-structure gradients using intrusive direct and adjoint methods. In a second part an alternative improved uncoupled non-intrusive approach is proposed. Both approaches are evaluated and compared on the Common Research Model (CRM) test-case considering criteria such as accuracy, efficiency, and applicability on practical industrial problem. Finally, preliminary results are presented on an inverse design problem. The final objective will be to match a target twist distribution on the Common Research Model wing using this new coupled gradient capability.

1 INTRODUCTION

The raise of composite materials in modern aircraft structures increases the structural flexibility of wings [1]. Consequently, fluid-structure interaction has to be considered when designing such flexible wings. With increasing computational resources, static aeroelastic simulations based on high-fidelity models are now commonly accessible and capable of tackling complex aeroelastic couplings. To improve the design of flexible wings, gradient based multi-disciplinary design optimization techniques are now effective and widely used [2–4]. However, gradients calculation is not trivial and can be costly when high-fidelity models are considered. Indeed, in an integrated optimization process, this difficulty increases for required cross-sensitivity derivatives such as the derivatives of aerodynamic performance with respect to structural sizes and derivatives of structural response with respect to changes in aerodynamic shape [5].

Several developments have been made over the last decade to compute aero-structure gradients using adjoint method [6–8]. At ONERA, active research work dedicated to aero-structure optimization was achieved during the past decade. In 2008, Marcelet [9] developed a module capable of computing static aeroelastic equilibrium and sensitivity analysis using adjoint method. However, the structural model behavior was limited to an equivalent beam model kinematics, and the aeroelastic gradients were only computed with respect to aerodynamic shape parameters. In a follow-on work, Ghazlane extended this work to take into account structural parameters (typically stiffener cross-section, plate thickness...) for aero-structure gradients computation [6]. Lastly, Viti [10] demonstrated a bi-step aero-structure preliminary design of a forward-swept wing applying these gradient computation tools. Nonetheless, the structural model was still limited to a beam model in all these works. Although useful for preliminary design studies and design space exploration, this structural modeling is not able to tackle complex aeroelastic couplings, nor deal with composite structures for efficient aeroelastic tailoring design, and is obviously limited to large aspect ratio wings.

The objective of a previous work [11] by the authors was to relieve all these limitations by re-developing an aero-structure gradient capability from scratch, by systematic hand differentiation of discretized aero-elastic equations, and all associated operators, in the ***elsA*** aeroelasticity module (***elsA***/Ael) [12]. This way, the new capability inherits the structural paradigm embedded into the ***elsA***/Ael module (structural flexibility matrix), the whole catalog of fluid-structure transfer methods, as well as the underlying parallel architecture. The equations and the solving procedure for the aeroelastic and the aero-structure gradients have been discussed in [11], where only aeroelastic gradients computation capability (i.e. gradients of aeroelastic functions of interest with respect to aerodynamic shape parameters) was available. This module, named ***elsA***/Aoc, has been recently extended in order to take into account structural design parameters in the direct and the adjoint mode.

The efficiency of the adjoint approach holds when a reduced number of responses is considered compared to a large set of design parameters. However, an industrial wing box sizing for preliminary design considers up to several hundreds of design parameters and up to several tens of thousands of structural constraints. In order to still benefit from the elegant adjoint formulation, some authors have proposed a constraint aggregation approach [13, 14] as an attempt to reduce the size of the set of admissible constraints, thus the number of gradients to compute. However, this technique has several drawbacks and may lead to sub-optimal designs. Considering these difficulties, the authors have proposed in a previous paper [15] a new strategy to compute high-fidelity aero-structure gradients (i.e. gradients of any function of interest with respect to structural design parameters). This strategy is based on an uncoupled non-intrusive approach benefiting from the linearized aerodynamic formulation. The main advantage of the method is the independency of the computational cost with respect to the number of constraints and potentially with respect to the number of structural design parameters. In addition this approach only requires rigid CFD computations.

The final objective of this work is to compare the efficiency of the uncoupled approach for aero-structure gradients computation, with the classical intrusive tangent or adjoint method, through the Common Research Model (CRM) wing design. The comparison aim at addressing the applicability of the optimization strategy on realistic industrial applications. Both approaches are investigated on the CRM test-case and criteria such as accuracy, efficiency and applicability on practical industrial problem are discussed.

The remainder of this paper is organized as follows: we first detail the intrusive direct and adjoint approaches. Then, an improved version of the non-intrusive method originally proposed in [15] is presented. Next, aero-structure gradients are computed on the CRM using these approaches. Finally, a strategy is proposed for an efficient structural sizing using high-fidelity aerostructure gradients, and preliminary results on the CRM wing are discussed.

The first theoretical parts presenting the two gradient computation methods have already been detailed in [16]. They are presented again to preserve the global consistency of this paper.

2 INTRUSIVE APPROACH

Let's assume that a steady aeroelastic equilibrium is available. In the following, we will denote the corresponding mesh as "flight shape", as opposed to the unloaded reference mesh called "jig shape". This is illustrated in Figure 1, where $\mathbf{X}_a$ is the equilibrium aerodynamic mesh, $\mathbf{X}_s$ the structural mesh, and $\mathbf{X}_{a0}$ the aerodynamic reference mesh. Our objective is to compute the sensitivity of a function of interest $\mathbf{J}$ with respect to a set of structural design variables $\mathbf{p}$ affecting the stiffness matrix only. To this end, direct and adjoint approaches derived from the linearization of the aeroelastic equations around the equilibrium position will be used.

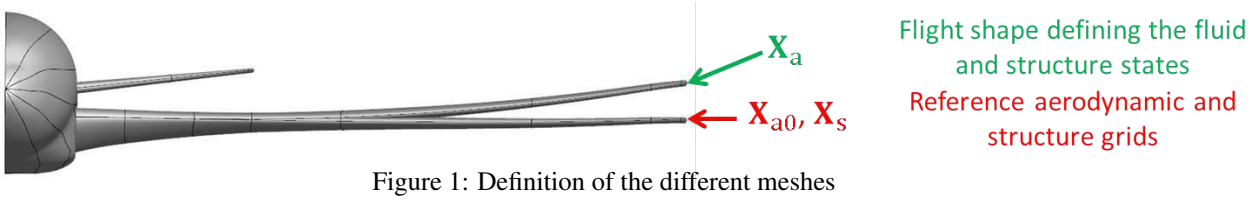

Figure 1: Definition of the different meshes

Let's denote the state variables of the coupled system $\mathbf{W}$ and $\mathbf{U}$, representing the fluid conservative variables and the structural displacements. At the aeroelastic equilibrium, the state variables and the meshes satisfy the discretized equations of fluid and structural mechanics simultaneously:

$$\begin{cases} \mathbf{R}_a(\mathbf{X}_a, \mathbf{W}, \mathbf{U}) = \mathbf{0} \\ \mathbf{R}_s(\mathbf{X}_s, \mathbf{W}, \mathbf{U}) = \mathbf{0} \end{cases} \tag{1}$$

with $\mathbf{R}_a$ and $\mathbf{R}_s$ a nonlinear and a linear system of discrete equations. These two blocks of equations are coupled through aerodynamic forces $\mathbf{Q}_a$ loading the structure skin and the structural displacements $\mathbf{U}$ deforming the fluid mesh. The structural loads $\mathbf{Q}_s$ are obtained with a suitable load transfer technique applied to $\mathbf{Q}_a$:

$$\mathbf{Q}_s(\mathbf{Q}_a(\mathbf{W}, \mathbf{X}_a), \mathbf{X}_{a0}, \mathbf{X}_s) = \mathbf{T}^Q_{surf}(\mathbf{X}_{a0}, \mathbf{X}_s)\mathbf{Q}_a(\mathbf{W}, \mathbf{X}_a) \tag{2}$$

where $\mathbf{T}^Q_{surf}(\mathbf{X}_{a0}, \mathbf{X}_s)$ represents the linear load transfer operator. The structural displacements alter the fluid grid positions through the relation:

$$\mathbf{X}_a = \mathbf{X}_{a0} + \delta\mathbf{X}_a(\delta\mathbf{X}_{a,surf}, \mathbf{X}_{a0}) = \mathbf{X}_{a0} + \mathbf{T}_{vol}(\mathbf{X}_{a0})\delta\mathbf{X}_{a,surf} \tag{3}$$

with $\mathbf{T}_{vol}(\mathbf{X}_{a0})$ the volume operator performing the deformation of the fluid interior domain. The vector $\delta\mathbf{X}_{a,surf}$ corresponds to the displacements of the fluid nodes at the aeroelastic interface:

$$\delta \mathbf{X}_{a,surf} = \delta \mathbf{X}_{a,surf}(\mathbf{X}_{a0}, \mathbf{X}_s, \mathbf{U}) = \mathbf{T}^U_{surf}(\mathbf{X}_{a0}, \mathbf{X}_s)\mathbf{U} \tag{4}$$

where $\mathbf{T}^U_{surf}(\mathbf{X}_{a0}, \mathbf{X}_s)$ represents the linear displacement transfer operator.

2.1 Direct approach

Let's consider the scalar aeroelastic objective function $J(\mathbf{W}, \mathbf{X}_a, \mathbf{X}_s)$ and a structural parameter p. We assume that the implicit function theorem is applicable to our problem. In this case, the state variables $\mathbf{W}$ and $\mathbf{U}$ can be expressed as implicit functions $\mathbf{W}(p)$ and $\mathbf{U}(p)$ of the optimization parameters and have the same properties of regularity than $\mathbf{R}_a$ and $\mathbf{R}_s$. Direct differentiation of system 1 with respect to p yields the tangent problem for the aero-structure gradient:

$$\begin{bmatrix} \dfrac{\partial \mathbf{R}_a}{\partial \mathbf{W}} & \dfrac{\partial \mathbf{R}_a}{\partial \mathbf{U}} \\ \dfrac{\partial \mathbf{R}_s}{\partial \mathbf{W}} & \dfrac{\partial \mathbf{R}_s}{\partial \mathbf{U}} \end{bmatrix} \begin{bmatrix} \dfrac{d\mathbf{W}}{dp} \\ \dfrac{d\mathbf{U}}{dp} \end{bmatrix} = \begin{bmatrix} -\dfrac{\partial \mathbf{R}_a}{\partial \mathbf{X}_a}\dfrac{d\mathbf{X}_a}{dp} \\ -\dfrac{\partial \mathbf{R}_s}{\partial \mathbf{X}_s}\dfrac{d\mathbf{X}_s}{dp} \end{bmatrix} \tag{5}$$

The resolution of this system makes the computation of the gradient of the objective function J possible:

$$\frac{dJ}{dp} = \frac{\partial J}{\partial \mathbf{W}}\frac{d\mathbf{W}}{dp} + \frac{\partial J}{\partial \mathbf{X}_a}\frac{d\mathbf{X}_a}{dp} + \frac{\partial J}{\partial \mathbf{X}_s}\frac{d\mathbf{X}_s}{dp} \tag{6}$$

Our objective is now to expand equations 5 and 6 only with respect to the unknown vectors $d\mathbf{W}/dp$ et $d\mathbf{U}/dp$. First, we remind that p affects only the stiffness of the structure, so that the following relations hold:

$$\frac{\partial \mathbf{X}_{a0}}{\partial p} = \frac{\partial \mathbf{X}_s}{\partial p} = \mathbf{0} \tag{7}$$

We then differentiate equation 3 with respect to p, and using equation 4, we get:

$$\frac{d\mathbf{X}_a}{dp} = \frac{d\delta \mathbf{X}_a}{dp} = \mathbf{T}_{vol}\mathbf{T}^U_{surf}\frac{d\mathbf{U}}{dp} \tag{8}$$

Substituting these two equations into 6 yields the expression of the total gradient of the objective function:

$$\frac{dJ}{dp} = \frac{\partial J}{\partial \mathbf{W}}\frac{d\mathbf{W}}{dp} + \frac{\partial J}{\partial \mathbf{X}_a}\mathbf{T}_{vol}\mathbf{T}^U_{surf}\frac{d\mathbf{U}}{dp} \tag{9}$$

Terms $\partial J/\partial \mathbf{X}_a$ and $\partial J/\partial \mathbf{W}$ only depend on the equilibrium steady state and are calculated analytically in a pre-processing step.

The structural residual can be written $\mathbf{K}(p)\mathbf{U}(p) - \mathbf{Q}_s(p) = \mathbf{0}$, where $\mathbf{K}$ is the stiffness matrix, and $\mathbf{Q}_s$ the structural loads. Using the functional dependency of the structural loads (see equation 2), the structural block reads:

$$\mathbf{K}\frac{d\mathbf{U}}{dp} = \mathbf{T}^Q_{surf}\left[\frac{\partial \mathbf{Q}_a}{\partial \mathbf{W}}\frac{d\mathbf{W}}{dp} + \frac{\partial \mathbf{Q}_a}{\partial \mathbf{X}_a}\frac{d\mathbf{X}_a}{dp}\right] - \frac{\partial \mathbf{K}}{\partial p}\mathbf{U} \tag{10}$$

The resolution of the coupled system 5 is done in an iterative way, alternatively on each block of equations. Using this last relation, system 5 can be cast into the compact form:

$$\begin{cases} \dfrac{\partial \mathbf{R}_a}{\partial \mathbf{W}}\dfrac{d\mathbf{W}}{dp}^{(k+1)} = -\dfrac{\partial \mathbf{R}_a}{\partial \mathbf{X}_a}[\mathbf{A}]\dfrac{d\mathbf{U}}{dp}^{(k)} \\ \\ \mathbf{K}\dfrac{d\mathbf{U}}{dp}^{(k+1)} = [\mathbf{B}]\dfrac{d\mathbf{W}}{dp}^{(k)} + [\mathbf{C}]\dfrac{d\mathbf{U}}{dp}^{(k)} - [\mathbf{D}]\mathbf{U} \end{cases} \tag{11}$$

Constant matrices $[\mathbf{A}]$,$[\mathbf{B}]$,$[\mathbf{C}]$ and $[\mathbf{D}]$ are defined analytically with the following formulas

$$\begin{aligned} [\mathbf{A}] &= \mathbf{T}_{vol}\mathbf{T}^U_{surf} \\ [\mathbf{B}] &= \mathbf{T}^Q_{surf}\frac{\partial \mathbf{Q}_a}{\partial \mathbf{W}} \\ [\mathbf{C}] &= [\mathbf{M}][\mathbf{A}] \\ [\mathbf{D}] &= \frac{\partial \mathbf{K}}{\partial p} \end{aligned} \tag{12}$$

where the utility matrix $[\mathbf{M}] = \mathbf{T}^Q_{surf}\dfrac{\partial \mathbf{Q}_a}{\partial \mathbf{X}_a}$ has been introduced.

The system in equation 11 is presented in a form suitable for an iterative block scheme resolution similar to the lagged-block strategy formely proposed in [17], superscript k being the current iteration number. Following the same notations, equation 9 becomes:

$$\frac{dJ}{dp} = \frac{\partial J}{\partial \mathbf{W}}\frac{d\mathbf{W}}{dp} + \frac{\partial J}{\partial \mathbf{X}_a}[\mathbf{A}]\frac{d\mathbf{U}}{dp} \tag{13}$$

2.2 Adjoint approach

In order to obtain the adjoint equations of the aero-structure gradient, the objective function is formulated by adding the total variation of the residuals $\mathbf{R}_a$ and $\mathbf{R}_s$ to dJ/dp. These variations with respect to the design variables being null, we then write for any vector $\mathbf{\Lambda}_a$ and $\mathbf{\Lambda}_s$:

$$\frac{dJ}{dp} = \frac{\partial J}{\partial \mathbf{W}}\frac{d\mathbf{W}}{dp} + \frac{\partial J}{\partial \mathbf{X}_a}[\mathbf{A}]\frac{d\mathbf{U}}{dp} + \mathbf{\Lambda}_a^T\frac{d\mathbf{R}_a}{dp} + \mathbf{\Lambda}_s^T\frac{d\mathbf{R}_s}{dp} \tag{14}$$

Expanding $d\mathbf{R}_a/dp$ and $d\mathbf{R}_s/dp$ and factorizing out the difficult terms $d\mathbf{W}/dp$ and $d\mathbf{U}/dp$ yields:

$$\begin{aligned}\frac{dJ}{dp} =& \left(\frac{\partial J}{\partial \mathbf{W}} + \mathbf{\Lambda}_a^T \frac{\partial \mathbf{R}_a}{\partial \mathbf{W}} - \mathbf{\Lambda}_s^T [\mathbf{B}] \right) \frac{d\mathbf{W}}{dp} \\ &+ \left(\frac{\partial J}{\partial \mathbf{X}_a} [\mathbf{A}] + \mathbf{\Lambda}_a^T \frac{\partial \mathbf{R}_a}{\partial \mathbf{X}_a} [\mathbf{A}] + \mathbf{\Lambda}_s^T (\mathbf{K} - [\mathbf{C}]) \right) \frac{d\mathbf{U}}{dp} + \mathbf{\Lambda}_s^T [\mathbf{D}] \mathbf{U}\end{aligned} \tag{15}$$

where adjoint vectors $\mathbf{\Lambda}_a$ and $\mathbf{\Lambda}_s$ are chosen such that the following system is satisfied:

$$\begin{bmatrix} \left[\frac{\partial \mathbf{R}_a}{\partial \mathbf{W}} \right]^T & -[\mathbf{B}]^T \\ [\mathbf{A}]^T \left[\frac{\partial \mathbf{R}_a}{\partial \mathbf{X}_a} \right]^T & \mathbf{K}^T - [\mathbf{C}]^T \end{bmatrix} \begin{bmatrix} \mathbf{\Lambda}_a \\ \mathbf{\Lambda}_s \end{bmatrix} = \begin{bmatrix} -\left[\frac{\partial J}{\partial \mathbf{W}} \right]^T \\ -[\mathbf{A}]^T \left[\frac{\partial J}{\partial \mathbf{X}_a} \right]^T \end{bmatrix} \tag{16}$$

Finally, once adjoint unknowns are determined, the total gradient is obtained with:

$$\frac{dJ}{dp} = \mathbf{\Lambda}_s^T [\mathbf{D}] \mathbf{U} = \mathbf{\Lambda}_s^T \frac{\partial \mathbf{K}}{\partial p} \mathbf{U} \tag{17}$$

Direct and adjoint equations have been written here for the particular case of a scalar aeroelastic function of interest (lift or drag coefficient), with optimization parameters controlling only the stiffness of the structure (e.g. stiffener cross-section, plate thickness). In a previous work by the authors [11], these equations have been detailed for the more general case of parameters affecting both the aerodynamic and the structure meshes. It is very interesting to note that the adjoint system 16 is exactly the same as the one presented in [11]. This means that this adjoint system is independent of the nature of the design parameter. Consequently, one resolution of this system gives access to the gradient of the aeroelastic function of interest with respect to all the parameters, regardless if they control aerodynamic shape, structural properties or even affect simultaneously stiffness and shape. Indeed, once the system is solved, the computational cost to obtain the gradient of the objective function with respect to these parameters is negligible. This constitutes a major advantage in the simultaneous optimization of both aerodynamic and structure.

3 NON-INTRUSIVE APPROACH

The non-intrusive technique allows a complete decoupling of the structure and the aerodynamic analysis. The idea consists in building a projection of the static displacement field on the structural modeshapes in order to re-use the rigid linearized kernel of the module ***elsA***/Opt. This approach has been discussed in [15]. With this strategy, aero-structure gradients have been computed on the ONERA M6 wing and then on the CRM configuration with satisfactory results. Both configurations used a RANS aerodynamic fluid model and a tridimensional FEM. In this section, after a brief reminder of the theory, some improvements are proposed to reach a better accuracy for the gradients.

3.1 Working process with the linearized solver

The linearized solver determines the perturbed field of conservative variables $\delta\mathbf{W}$ with respect to the steady state flow, when the fluid domain boundary is perturbed by a prescribed displacement induced by a perturbation of a structural design parameter δp. The corresponding perturbed structural loads $\delta\mathbf{Q}_s$ are then deduced directly from the solution $\delta\mathbf{W}$.

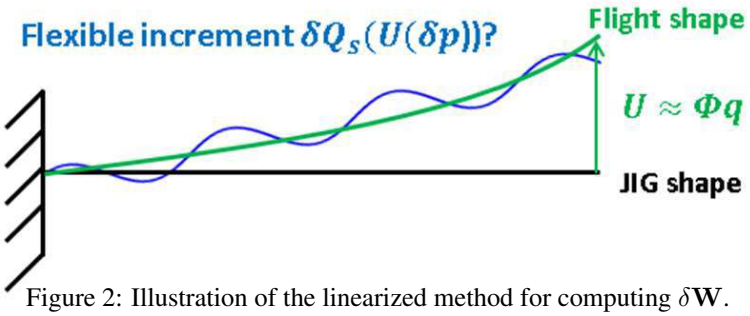

Figure 2: Illustration of the linearized method for computing $\delta\mathbf{W}$.

This process is illustrated in Figure 2. Flexibility is taken into account into the steady solution and the computation of $\delta\mathbf{W}$ is performed by a linearization around the equilibrium mesh position denoted *Flight shape*.

Let's consider the tangent system 11. Solving for the first block of equations and substituting $d\mathbf{W}/dp$ in the structure block yields:

$$\begin{cases} \big(\mathbf{K} - [\mathbf{Z}]\big)\dfrac{d\mathbf{U}}{dp} = -\dfrac{\partial \mathbf{K}}{\partial p}\mathbf{U} \\ \\ [\mathbf{Z}] = -[\mathbf{B}]\left[\dfrac{\partial \mathbf{R}_a}{\partial \mathbf{W}}\right]^{-1}\dfrac{\partial \mathbf{R}_a}{\partial \mathbf{X}_a}[\mathbf{A}] + [\mathbf{D}] \end{cases} \tag{18}$$

$\big(\mathbf{K} - [\mathbf{Z}]\big)$ appearing in the first block of system 18 is the Schur complement of the matrix block $\partial \mathbf{R}_a/\partial \mathbf{W}$. We remind that direct differentiation of the static equation $\mathbf{KU} = \mathbf{Q}_s$ with respect to p gives:

$$\frac{\partial \mathbf{K}}{\partial p}\mathbf{U} + \mathbf{K}\frac{d\mathbf{U}}{dp} = \frac{d\mathbf{Q}_s}{dp} \tag{19}$$

Comparing this expression with the first block of equation in system 18 yields the relation:

$$\frac{d\mathbf{Q}_s}{dp} = [\mathbf{Z}]\frac{d\mathbf{U}}{dp} \tag{20}$$

where $[\mathbf{Z}]$ is the kernel matrix of the linearized flow solver.

3.2 Modal reconstruction of aero-structure gradients from an aeroelastic configuration

Let's consider the steady equilibrium corresponding to a fluid state $\mathbf{W}$, a mesh position $\mathbf{X}_a$ and a structural displacement field $\mathbf{U}$:

$$\mathbf{KU} = \mathbf{Q}_s = [\mathbf{T}^Q_{surf}]\mathbf{Q}_a(\mathbf{W}, \mathbf{X}_a) \tag{21}$$

$\mathbf{K}$ is the stiffness matrix of the finite element model, $\mathbf{Q}_s$ the nodal structural loads, $\mathbf{Q}_a$ the aerodynamic loads computed on the aerodynamic skin. If the full set $\mathbf{\Phi}$ of structural eigenvectors was available, the modal projection $\mathbf{U} = \mathbf{\Phi q}$ would hold exactly. Then substituting in equation 21 gives the corresponding generalized coordinates as:

$$\mathbf{q} = \boldsymbol{\gamma}^{-1}\mathbf{\Phi}^T\mathbf{Q}_s \tag{22}$$

where $\boldsymbol{\gamma} = \mathbf{\Phi}^T\mathbf{K}\mathbf{\Phi}$ denotes the diagonal generalized stiffness matrix. In practice only a restricted set of first $n_{\mathbf{\Phi}}$ eigensolutions is computed and the modal approximation to $\mathbf{U}$ becomes:

$$\mathbf{U} \approx \mathbf{U}_\Phi = \sum_{i=1}^{n_\Phi} \mathbf{\Phi}_i q_i \tag{23}$$

However, remind that $\mathbf{U}$ is computed exactly from equation 21 such that the residual term in equation 23 is known from the simple difference $\mathbf{U}_{res} = \mathbf{U} - \mathbf{U}_\Phi$. Equation 21 can now be reformulated as

$$\mathbf{K}(\mathbf{U}_\Phi + \mathbf{U}_{res}) = \mathbf{Q}_s \tag{24}$$

Inserting the modal decomposition of $\mathbf{U}$ in the expression of the gradient of structural loads (equation 20) leads to

$$\frac{d\mathbf{Q}_s}{dp} = \mathbf{Z}(\mathbf{\Phi}\frac{d\mathbf{q}}{dp} + \frac{\partial\mathbf{\Phi}}{\partial p}\mathbf{q}) + \mathbf{Z}\frac{\partial\mathbf{U}_{res}}{\partial p} \tag{25}$$

The use of partial derivatives in the equation above means that $\mathbf{\Phi}$ and $\mathbf{U}_{res}$ only depend on p. This latter assumption is valid if $\mathbf{U}_{res}$ is considered as a static residual mode (i.e. a structural displacement under an assumed prescribed load case). In order to exploit this relation, the gradient of the generalized coordinates has to be determined. With some algebra manipulation, it is possible to demonstrate that:

$$\frac{d\mathbf{q}}{dp} = [\boldsymbol{\gamma} - \mathbf{GAF}]^{-1}\left(-\frac{\partial\boldsymbol{\gamma}}{\partial p}\mathbf{q} + \mathbf{\Phi}^T\mathbf{Z}(\frac{\partial\mathbf{\Phi}}{\partial p}\mathbf{q} + \frac{\partial\mathbf{U}_{res}}{\partial p})\right) \tag{26}$$

where the generalized aerodynamic forces matrix is defined as $\mathbf{GAF} = \mathbf{\Phi}^T\mathbf{Z}\mathbf{\Phi}$.

The computational cost of this method can be easily determined with a reformulation of equation 25:

$$\frac{d\mathbf{Q}_s}{dp} = \mathbf{Z}\mathbf{\Phi}\frac{d\mathbf{q}}{dp} + \mathbf{Z}(\frac{\partial\mathbf{\Phi}}{\partial p}\mathbf{q} + \frac{\partial\mathbf{U}_{res}}{\partial p}) \tag{27}$$

The first part ($\mathbf{Z}\mathbf{\Phi}$) of equation 27 costs one linearized computation per mode. The second part ($\mathbf{Z}(\frac{\partial\mathbf{\Phi}}{\partial p}\mathbf{q} + \frac{\partial\mathbf{U}_{res}}{\partial p})$) requires one linearized computation per parameter. Once these two parts are determined, the gradient of the generalized coordinates is readily available.

Usually, few mode shapes are necessary to correctly approximate the structural displacements (equation 24), however many design variables can be defined in the optimization problem. In

this case, the method loses interest since it is independent of the number of objective functions, but dependent on the number of design variables. In an attempt to reduce the computational cost, gradients can be approximated by dropping the terms which depend on design variable number. In this case equations 26 and 27 become:

$$\frac{d\mathbf{q}}{dp} = [\boldsymbol{\gamma} - \mathbf{GAF}]^{-1}\left(- \frac{\partial \boldsymbol{\gamma}}{\partial p}\mathbf{q}\right) \tag{28}$$

$$\frac{d\mathbf{Q}_s}{dp} = \mathbf{Z}\boldsymbol{\Phi}\frac{d\mathbf{q}}{dp} \tag{29}$$

4 CRM TEST-CASE

In this section, we apply the intrusive and non-intrusive approaches to the CRM. Our objective is to compute lift and pressure drag coefficient sensitivities with respect to structural parameters, as well as gradients of structural loads. The aerodynamic skin of the selected wing/body/HTP (WBH) configuration is depicted in Figure 3. For all subsequent results, a RANS fluid model is used with an upwind Roe scheme and a MUSCL interpolation associated to a Van Albada limiting function. The Spalart-Allmaras one-equation turbulence model is selected. In the attempt to find a lift coefficient of 0.5 for a Mach number of 0.85 at 35000 ft, an angle of attack of 2.127 is applied.

Several finite element models of the CRM wing are available on the NASA CRM website. All these models correspond to the flight shape of the CRM. The model V14 exhibits an expected static behavior, with a realistic vertical displacement of 2.15 m observed at the wing tip in nominal cruise conditions. It is a simple finite element model of the wing box and centre box with spars, skins, ribs, implicit stiffeners and a constant wing skin thickness of 8.89 mm. This model can be considered as a good starting point for a structural sizing process. The provided CRM configuration corresponds to the 1 g cruise shape. In order to find the corresponding jig shape, an inverse procedure has been set up and presented in [15]. To correctly predict the structural displacement due to gravity, a realistic distribution of concentrated masses representing the fuel in the wing is added, along with concentrated masses for the engine, pylon and landing gear. Figure 3 presents the finite element model colored by the structural optimization groups, along with the aerodynamic skin of the CRM. Ten structural parameters are defined, split into two groups of five parameters driving the thickness of the lower skin and the upper skin respectively. In the following, the results will be presented only for the lower skin (see Figure 4), since for this exercise upper and lower skin have the same thickness distribution.

The first nine eigenmodes computed on the initial FEM of the CRM wingbox and smoothed on the aerodynamic skin are presented in Figure 5. As detailed in [15], twenty modes will be used to compute the gradients with the non-intrusive approach.

For the intrusive approach, the convergence of the discrete residual norm of the fluid block is reported in Figure 6. In direct mode, five right hand sides are considered, i.e. one for each design parameter. In adjoint mode, two right hand sides are considered, that is one for each objective function.

Tables 1 and 2 summarize the total lift and drag coefficient derivatives respectively, and allows a comparison between intrusive and non-intrusive approach. Gradients obtained with the

tangent approach, taken as reference here, have been validated with finite difference results on an other test-case in [16]. The very low discrepancies observed between tangent and adjoint approach demonstrate that the duality between the two methods is numerically satisfied. These results validate for this test-case the implementation of the direct and adjoint method into ***elsA*** for gradients of aeroelastic function of interest with respect to structural design variables. The non-intrusive approach with and without the eigenvector derivatives contribution ($\partial\mathbf{\Phi}/\partial p$) gives satisfactory results, since the sign and the order of magnitude are always well predicted compared to the intrusive approach. We remind that without this contribution, the method is independent of the number of design variables, reducing dramatically the computational cost of the gradients.

For the particular case of aeroelastic coefficient derivatives with respect to structural parameters, there are usually few objective functions but many design variables. Therefore, the adjoint method is the preferable approach, since it requires to solve the adjoint system 16 only once per objective function.

Now considering the total derivatives of the structural loads, the computational cost of the adjoint approach is indexed to the number of individual force components. Usually, a realistic structural loading consists in up to several hundreds of individual force components. This is

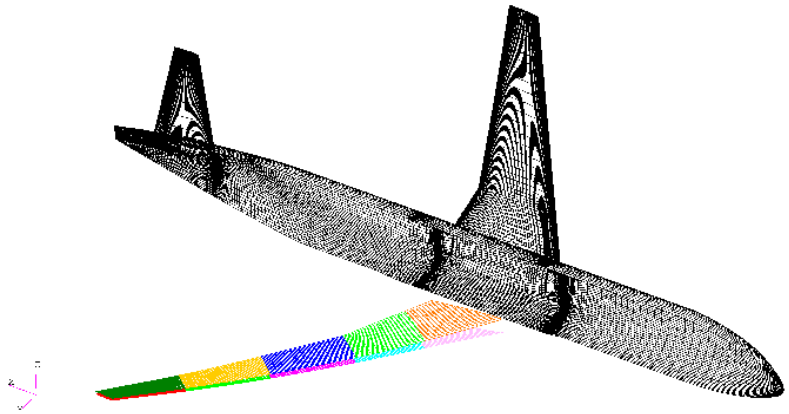

Figure 3: FEM colored by structural optimization group, along with the CRM aerodynamic skin.

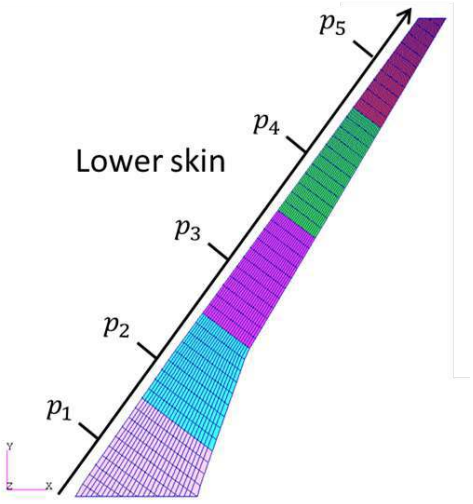

Figure 4: First five structural design parameters.

comparable to the typical number of design parameters for a realistic optimization process. In this context, none of the tangent or adjoint method really stands out. However, computing the gradients of structural loads using the non-intrusive approach but without the eigenvector derivatives contribution requires significant lower computational cost, compared to the intrusive approaches. Again, in this case, aero-structure gradients only cost one rigid linearized computation per mode shape.

In order to assess the accuracy of the non-intrusive approach, total derivatives of the structural loads are computed with the tangent approach and compared to the non-intrusive approach (with and without eigenvector derivatives). To have a representative example, gradients of horizontal and transverse forces with respect to p_1 and p_4 are considered. For sake of clarity, normalized

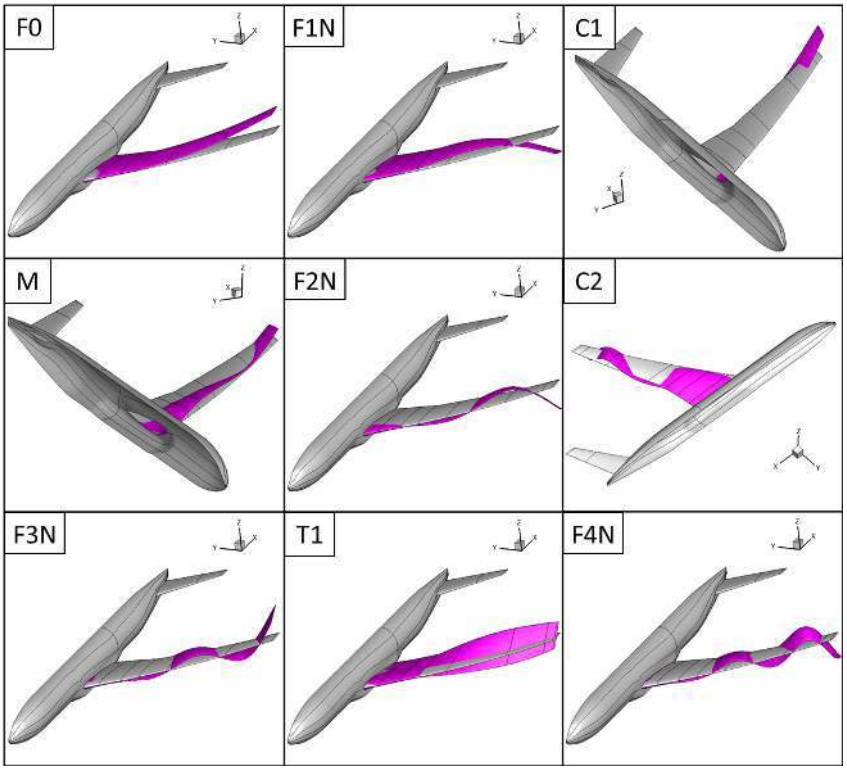

Figure 5: First nine structural mode shapes splined on the wetted surface.

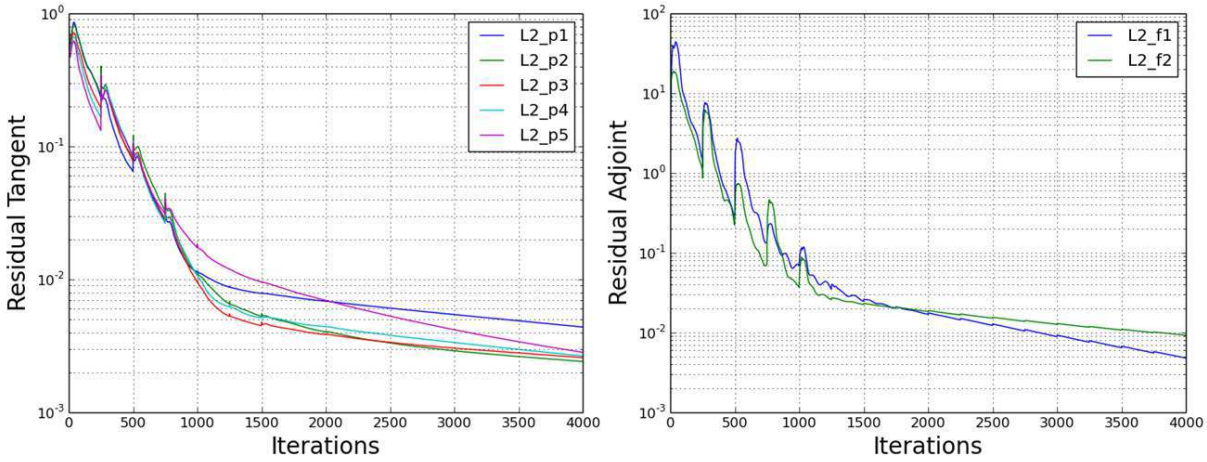

Figure 6: Convergence of linear gradient density residual for five parameters (left) and adjoint residual for two objective functions (right).

		Intrusive		Non-Intrusive	
		Direct	Adjoint	$\mathbf{\Phi}$, $\partial\mathbf{\Phi}/\partial p$	$\mathbf{\Phi}$
dC_l/dp	p_1	$+3.993 \times 10^{-3}$	$+4.028 \times 10^{-3}$	$+3.186 \times 10^{-3}$	$+4.624 \times 10^{-3}$
	p_2	$+1.200 \times 10^{-2}$	$+1.209 \times 10^{-2}$	$+1.112 \times 10^{-2}$	$+9.274 \times 10^{-3}$
	p_3	$+7.682 \times 10^{-3}$	$+7.728 \times 10^{-3}$	$+8.467 \times 10^{-3}$	$+8.290 \times 10^{-3}$
	p_4	$+2.019 \times 10^{-3}$	$+2.018 \times 10^{-3}$	$+2.580 \times 10^{-3}$	$+2.449 \times 10^{-3}$
	p_5	$+1.202 \times 10^{-4}$	$+1.193 \times 10^{-4}$	$+1.545 \times 10^{-4}$	$+2.748 \times 10^{-4}$

Table 1: Gradients for lift coefficients with respect to wing skin thicknesses.

		Intrusive		Non-Intrusive	
		Direct	Adjoint	$\mathbf{\Phi}$, $\partial\mathbf{\Phi}/\partial p$	$\mathbf{\Phi}$
dC_d/dp	p_1	$+2.262 \times 10^{-4}$	$+2.287 \times 10^{-4}$	$+1.844 \times 10^{-4}$	$+2.420 \times 10^{-4}$
	p_2	$+6.578 \times 10^{-4}$	$+6.640 \times 10^{-4}$	$+6.105 \times 10^{-4}$	$+4.763 \times 10^{-4}$
	p_3	$+3.592 \times 10^{-4}$	$+3.620 \times 10^{-4}$	$+3.944 \times 10^{-4}$	$+4.221 \times 10^{-4}$
	p_4	$+8.034 \times 10^{-5}$	$+8.000 \times 10^{-5}$	$+1.061 \times 10^{-4}$	$+1.260 \times 10^{-4}$
	p_5	$+4.960 \times 10^{-6}$	$+4.983 \times 10^{-6}$	$+8.612 \times 10^{-6}$	$+1.404 \times 10^{-5}$

Table 2: Gradients for drag coefficients with respect to wing skin thicknesses.

gradients are plotted on nodes belonging to the front spar only (see Figures 7-10). First of all, results for intrusive and non-intrusive approach qualitatively match pretty well. Taking the intrusive approach as reference, it is observed that the non-intrusive approach is always predictive when eigenvector derivatives contribution is added. Gradients computed with respect to p_1 without eigenvector derivatives are still close to the reference values. However, those computed with respect to p_4 are either inaccurate or wrong. This points out the relevancy of considering the eigenvector derivatives for some design variables. In [15], the authors propose a criterion that measures the amount of relevant information contained in the eigenvector derivatives compared to the information contained in the modal basis. It reveals whether a specific parameter requires the addition of eigenvector derivatives in the load sensitivity reconstruction. Nevertheless, it can be observed that these discrepancies occur mainly for low-valued gradients, which do not significantly affects gradient-based optimization since the optimizer's path is mostly driven by high-valued sensitivities.

5 STRUCTURAL SIZING OF THE CRM WING USING HIGH-FIDELITY AERO-STRUCTURE GRADIENTS

5.1 Force approximation method

High-fidelity structural sizing requires derivatives of structural responses (typically constraints) with respect to structural parameters. These derivatives are costly, even when computed with the adjoint method since it requires as many resolution of the adjoint system as the total number of constraints in the whole structure. In an attempt to reduce the size of the set of admissible

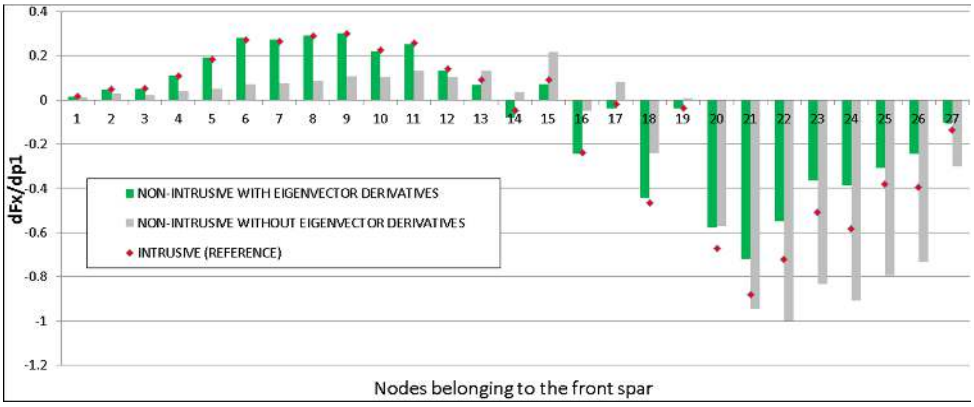

Figure 7: Gradients of horizontal force with respect to p_1, computed with the non-intrusive approach (green and grey bars). Reference tangent approach values (red markers) are provided.

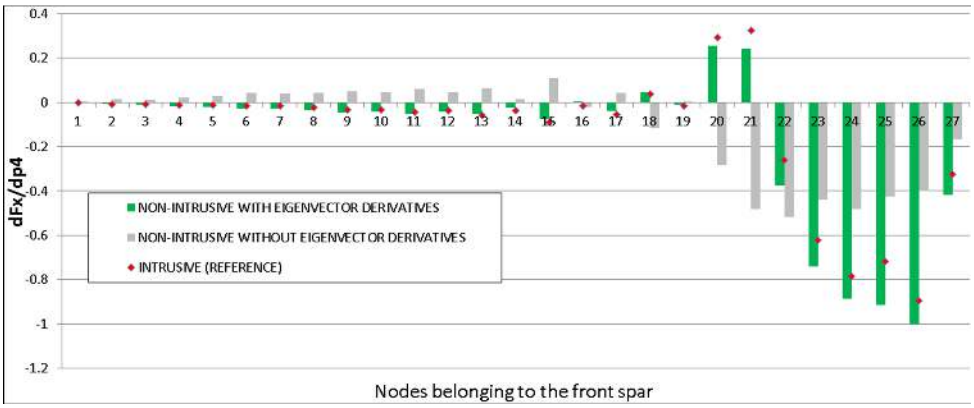

Figure 8: Gradients of horizontal force with respect to p_4, computed with the non-intrusive approach (green and grey bars). Reference tangent approach values (red markers) are provided.

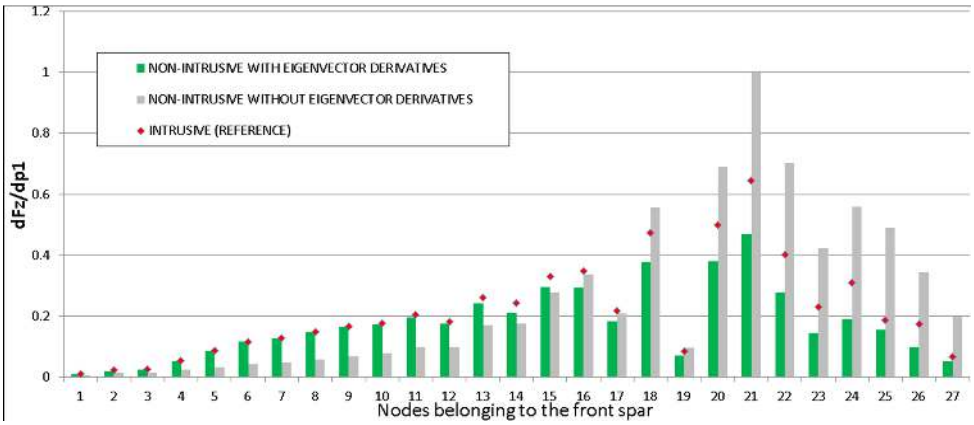

Figure 9: Gradients of transverse force with respect to p_1, computed with the non-intrusive approach (green and grey bars). Reference tangent approach values (red markers) are provided.

constraints, thus the number of gradients to compute, some authors have proposed to use a constraint aggregation approach in conjunction with the adjoint method. As already mentioned, this approach has several drawbacks and needs to be tuned appropriately.

Approximating constraint responses is not easy, since they may exhibit irregular distribution in the structure. In contrast, the structural loads are easier to approximate due to their smoother distribution. It is therefore proposed to use the force approximation method [18] as an alternative to a constraint aggregation approach. Assuming a general linear elastic behavior, the relationship

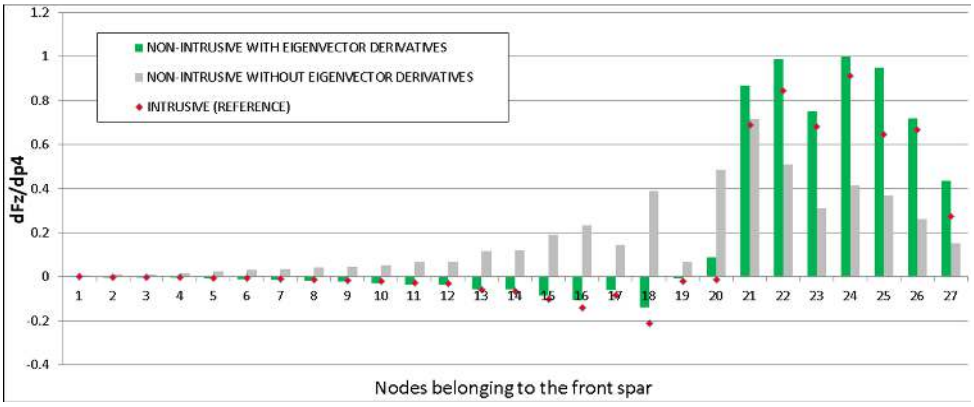

Figure 10: Gradients of transverse force with respect to p_4, computed with the non-intrusive approach (green and grey bars). Reference tangent approach values (red markers) are provided.

between stresses and strains would be linear of the form $\sigma = \mathbf{H}(\epsilon - \epsilon_0) + \sigma_0$, where $\mathbf{H}$ denotes the elasticity matrix and ϵ_0 and σ_0 the initial strain and stress fields. The deformation field is obtained from the nodal displacements through the usual relation $\epsilon = \mathbf{SNU(p)} = \mathbf{BU(p)}$, $\mathbf{S}$ being a linear differential operator and $\mathbf{N}$ the matrix of shape functions. Direct differentiation of σ with respect to a scalar structural parameter p yields:

$$\frac{d\sigma}{dp} = \frac{\partial\sigma}{\partial\mathbf{U}}\frac{d\mathbf{U}}{dp} = \mathbf{HB}\frac{d\mathbf{U}}{dp} \tag{30}$$

Deriving the static equation $\mathbf{KU} = \mathbf{Q}_s$ with respect to p gives the expression of the structural displacement derivatives:

$$\frac{d\mathbf{U}}{dp} = -\mathbf{K}^{-1}\frac{\partial\mathbf{K}}{\partial p}\mathbf{U} + \mathbf{K}^{-1}\frac{d\mathbf{Q}_s}{dp} \tag{31}$$

Equation 30 becomes:

$$\frac{d\sigma}{dp} = \mathbf{HBK}^{-1}\left(-\frac{\partial\mathbf{K}}{\partial p}\mathbf{U} + \frac{d\mathbf{Q}_s}{dp}\right) = \frac{d\sigma_U}{dp} + \frac{d\sigma_Q}{dp} \tag{32}$$

where $d\sigma_U/dp$ is a constraint response under a standard static pseudo-load $\mathbf{F}_U = -(\partial\mathbf{K}/\partial p)\mathbf{U}$, and $d\sigma_Q/dp$ is a constraint response under the pseudo-load $\mathbf{F}_Q = d\mathbf{Q}_s/dp$. Therefore, for each static load $\mathbf{Q}_s$, a companion load $d\mathbf{Q}_s/dp$ must be defined. With this strategy, the total gradient of a constraint response can be recombined from two separate standard static sensitivity analyses. However, we adopt an even simpler approach by directly providing a linear approximation of the aeroelastic loads to the structure optimizer. Given a structural parameter p varying around its current value p_0, and knowing the load vector total derivative, we simply formulate the linear approximation:

$$\mathbf{Q}_s(p) \approx \mathbf{Q}_s(p_0) + \frac{d\mathbf{Q}_s}{dp}\delta p \tag{33}$$

Then by linearity assumption the total gradient of the constraints is directly obtained, leaving the computational burden to the structure solver.

5.2 Proposed strategy for an efficient structural sizing

Given a Finite Element Model (FEM) of the CRM wing and the associated fluid mesh, our objective is to match a target twist distribution extracted from the original geometry of the CRM wing (see [19]). This inverse design problem can be formulated as:

$$\text{Minimize } J(\mathbf{p}) \text{ such that: } \begin{cases} J(\mathbf{p}) = \sum_{i=1}^{N} \left(\frac{U_i^T - U_i(\mathbf{p})}{U_i^T} \right)^2 \\ \boldsymbol{\epsilon}(\mathbf{p}) \leq \boldsymbol{\epsilon}_{max} \\ \mathbf{p}_{min} \leq \mathbf{p} \leq \mathbf{p}_{max} \end{cases} \tag{34}$$

where $\mathbf{U}^T$ is a set of target displacements leading the initial structural mesh to the desired shape. The structure is assumed to be manufactured from Aluminum 2024. The corresponding limit allowable stress is $\boldsymbol{\sigma}_{max} = 324MPa$, from which the corresponding maximum allowable strain $\boldsymbol{\epsilon}_{max}$ is derived. The set of structural parameters $\mathbf{p}$ is defined as the thickness of 27 structural groups depicted in Figure 11. Eleven parameters control the lower and upper skins, ten parameters the front and rear spars, and five parameters the stringers.

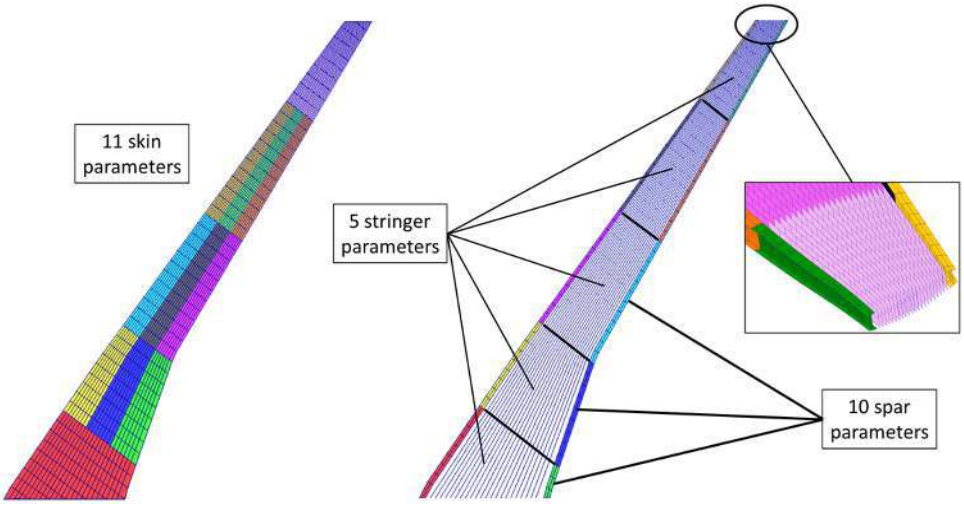

Figure 11: Structural design parameters used to size the structure.

The optimization process depicted in Figure 12 relies on the aerodynamic software ***elsA*** for the computation of aeroelastic loads and associated gradients, and on the MSC NASTRAN software for the structural analysis and optimization part. The process has two levels of convergence: one at the upper level on the load cases and one at the optimizer level on physical properties and design objective function. The structural optimization process is converged for a given set of external non-linear aeroelastic loads. In this optimization cycle the complete FEM is used and the optimization parameters are the physical properties of various structural members. Then, an equivalent reduced order model (flexibility matrix) of the sized structural model is automatically derived in order to perform the adequate flexible static aeroelastic computations at the current iteration. Once the new flexible non-linear loads are obtained, they are transferred to the structural grid and a new optimization process is performed. This organization is very flexible as it does not require any modification to the NASTRAN core solver.

Figure 12 presents different optimization processes to solve problem 34, according to the strategy chosen to compute the loads. If they come from Doublet Lattice Method (DLM) only (first case), then the optimization strategy merely relies on standard NASTRAN capabilities. The second case named "DLM+Correction" corresponds to the DLM prediction corrected by data from rigid CFD, thus requiring off-line ***elsA*** aerodynamic computations. The third case is based on an external CFD based Aeroelastic Analysis (A.A.) to estimate the loads. Thus, at each external iteration, the flexibility matrix $\mathbf{S}$ (which ensures the fluid/structure coupling such that $\mathbf{U} = \mathbf{S}\mathbf{Q}_s$) and the displacements due to gravity have to be updated. These aerodynamic loads are kept constant during the internal optimization loop. Finally, the last case extends the previous one with the contribution of load sensitivities computed with ***elsA*** (Aeroelastic + Sensitivity Analysis). The optimizer benefits from the additional contribution of the linearized loads using the force approximation method.

In the first two cases, a strong coupling exists between the aerodynamic and the structural discipline, but the fidelity of the fluid model is low. For the last two cases, of higher-fidelity, there is a weak coupling between these two disciplines, since the loads and their sensitivities are not updated at each re-analysis of the FEM.

A strategy based on a strong coupling and high-fidelity models would involve the merge between the re-analysis loop and the external loads loop. Consequently, for each re-analysis asked by the structural optimizer, ***elsA*** would be invoked to compute the loads and their sensitivities for the current set of structural parameters and to provide them to the NASTRAN optimizer. In scheme 12, this means to replace the 20 re-analysis per external iteration by only one re-analysis per external iteration. However, this strategy is expected to be of higher computational cost.

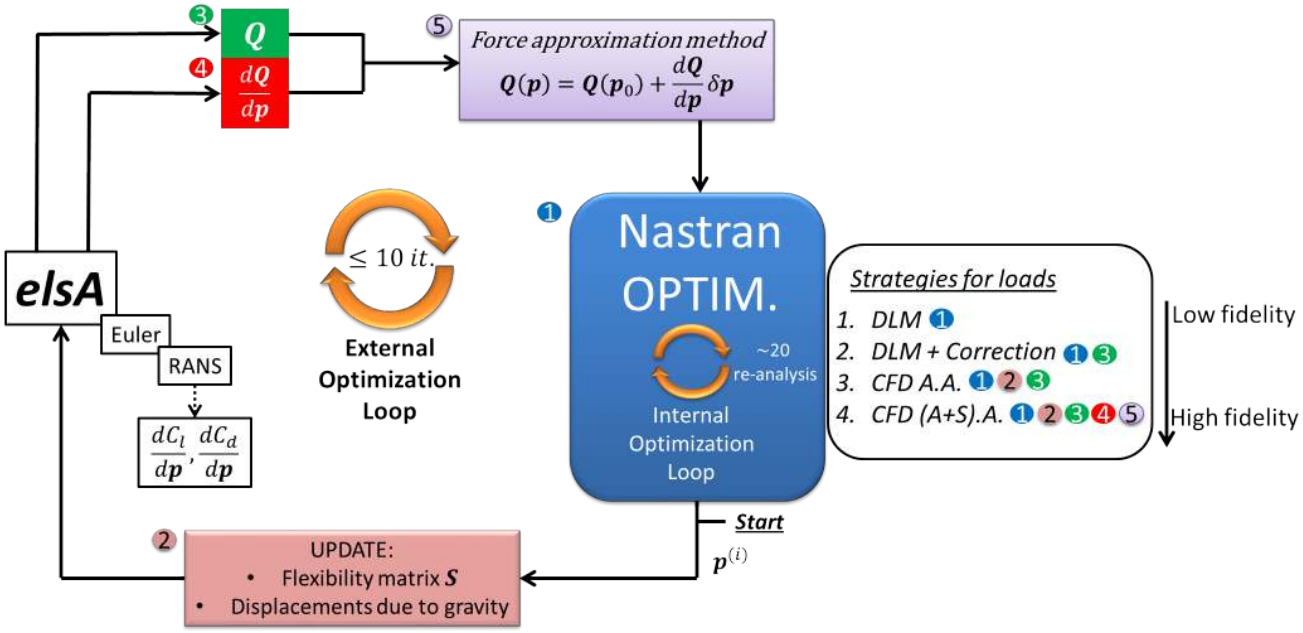

Figure 12: Structural optimization strategy.

As explained in section 4, the non-intrusive approach provides an efficient way to access gradients of loads. However, for cross-gradients like aerodynamic coefficient derivatives with respect to structural parameters, the adjoint method is preferable. With both capabilities readily available, an aerodynamic performance monitoring can be achieved during the sizing process,

particularly by taking into account $dC_d/d\mathbf{p}$ or $dC_l/d\mathbf{p}$ into the optimization.

Last but not least, a strong advantage of treating the sizing process with separate aerodynamic and structural parts lies in the possibility to use an adapted fluid mesh according to the purpose of the simulation. When gradients of loads are needed, then a Euler mesh might be accurate enough. In contrast, to estimate drag coefficient derivatives, a RANS mesh is more appropriate (see Figure 12). This flexibility for the computation of the different terms is beneficial to save CPU time.

5.3 Preliminary results

In this section, first results on the optimization problem exposed above are presented and discussed. The strategy chosen is based on a weak coupling, and the loads are updated with high-fidelity aeroelastic analysis at each external iteration. For these preliminary results, load sensitivities are not taken into account, which corresponds to the third case in Figure 12. This strategy is similar to that presented in [20]. Only one load case is considered for this application, referring to the 1 g cruise flight. The optimization method used in the NASTRAN SOL 200 is the Modified Method of Feasible Directions (MMFD, [21]).

Figure 13 plots the objective function value with respect to the re-analysis number. For each external iteration, twenty FE re-analysis are performed, and there are ten external iterations. Every FE re-analysis loop begins with an evaluation of the objective function. In order to do this, the updated loads are applied on the previous optimal configuration. These evaluations generate the "peaks" noticeable every 21 iterations, resulting from the loads dependency to the structural design variables. The value of those peaks decrease in such a way that after the eighth external iteration, no peak is observable. Thus, the loads are no longer varying significantly between two external iterations. This situation indicates that the optimization process was able to size the structure using realistic loads. Indeed, the sizing loads are in accordance to those computed with the final design.

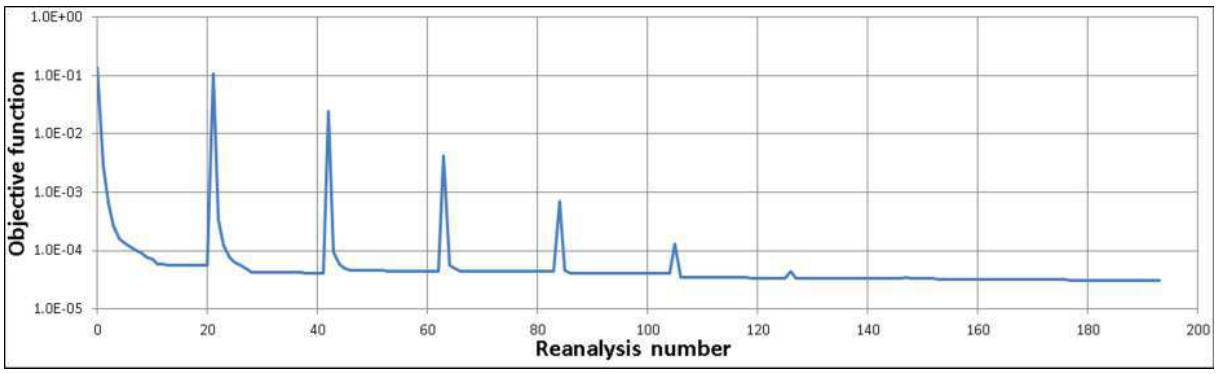

Figure 13: Structural optimization convergence.

Figure 14 plots the twist laws obtained for the first, the second and the last external iteration respectively. The black line corresponds to the initial twist law generated with the updated loads applied on the former optimum point (before the twenty reanalysis). The blue twist law is obtained with the same loads but this time applied on the optimized structure (end of the twenty reanalysis). Finally, the red line is the target twist law. For each iteration, a good agreement is found between the blue (optimized) twist law and the target twist law. Naturally, the black (initial) twist law has the same behavior as the peaks from Figure 13: the discrepancies between

this twist law and the target one decrease while the external iteration number increases, until a perfect matching at the end of the external optimization loop.

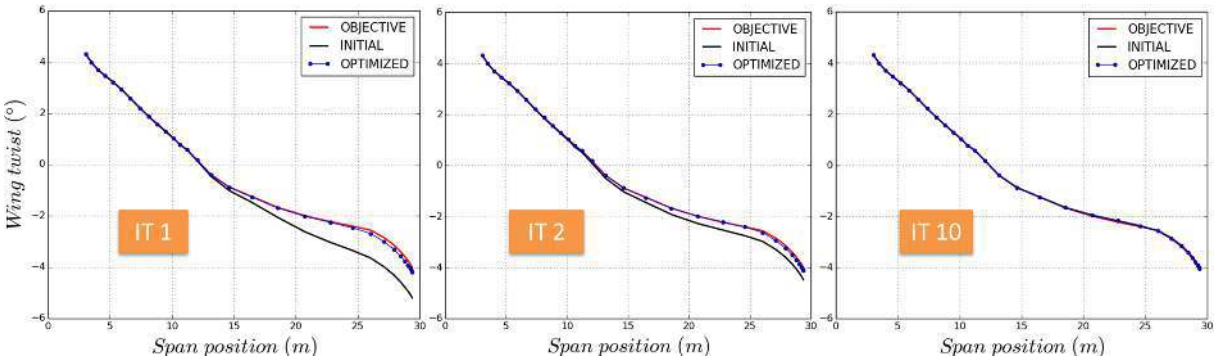

Figure 14: Initial (black), optimized (blue) and target (red) twist laws for three external iterations.

This simple application proves the effectiveness of the strategy proposed to solve the inverse design problem. A more complex optimization will be set up soon, taking into consideration multiple load cases and, obviously, introducing the gradients into the process.

6 CONCLUSIONS

In this paper two approaches are presented to compute high-fidelity aero-structure gradients. The first one is based on the classical intrusive direct and adjoint approaches, and the second one is an uncoupled non-intrusive method benefiting from the linearized aerodynamic theory. Total derivatives of structural loads, and lift and drag coefficients, with respect to structural design parameters, are computed on the Common Research Model test-case, using both intrusive and non-intrusive approaches.

Gradients obtained with the tangent approach are taken as reference since it has been validated previously on an other test-case [16]. The very low discrepancies observed between direct and adjoint approach demonstrate that the duality between the two methods is preserved. These results validate the implementation of the direct and adjoint method into ***elsA*** for gradients of aeroelastic function of interest with respect to structural design variables.

The non-intrusive reconstruction gives satisfactory results compared to the other approaches. The strength of this approach relies on its potential low computational cost, but cannot overcome the adjoint method for the particular case of aerodynamic coefficient derivatives. However, it represents a very promising alternative to compute gradients of structural loads for structural sizing. Usually, for this purpose, constraint aggregation technique is used in conjunction with the adjoint method. However, limiting the number of stress responses in the sizing process may oversimplify the problem formulation, leading to poor designs. In contrast, considering a limited number of structural loads can still lead to a realistic load path and then to a predictive set of stress responses. This is obviously in favor of the direct approach which in this case exhibits a comparable cost to the adjoint approach. We remind that computing the gradients of structural loads using the non-intrusive approach without the eigenvector derivatives contribution requires only one linearized computation per mode shape. Satisfactory results have been obtained on the CRM test-case by applying this approximation. In addition, this method provides aero-structure gradients with only rigid linearized aerodynamic computations, which is interesting for those who do not have access to strongly coupled aero-structure tangent or adjoint solver. Finally,

uncoupled approaches are very interesting for MDO teams autonomy, which is a determining advantage in an industrial optimization process.

Ultimately, an inverse design problem is presented, with the objective to match a target twist law on the CRM wing. A strategy is proposed for an efficient structural sizing using high-fidelity aero-structure gradients. This strategy is based on the force approximation method, considered as an alternative to a constraint aggregation approach. Indeed, due to their smoother distribution, the structural loads are easier to approximate than the stresses. Several optimization processes are envisaged, according to the strategy selected to compute the loads. Preliminary results are presented on a weak coupling strategy, where the loads are updated with high-fidelity aeroelastic analysis at each external iteration. For these first results, load sensitivities are not taken into account. Nevertheless, it is demonstrated that the target twist law is reached after few external iterations, with the aeroelastic loads corresponding to the actual design. It is expected that this number of iterations will decrease with the additional contribution of the load derivatives.

The final objective of this work is to compare the intrusive adjoint method and the non-intrusive uncoupled approach through the inverse design problem described previously. The comparison will address the applicability of the optimization strategy on realistic industrial applications, in terms of efficiency and accuracy.

7 REFERENCES

[1] Weisshaarr, T. A. (1980). Divergence of forward swept composite wings. *Journal of Aircraft*, 17.6, 442–448.

[2] Kenway, G. K. W., Kennedy, G. J., and Martins, J. R. R. A. (2014). Aerostructural optimization of the common research model configuration. In *15th AIAA/ISSMO Multidisciplinary Analysis and Optimization Conference*.

[3] Jameson, A. (2010). Aerodynamic-structural design studies of low-sweep transonic wings. *JOURNAL OF AIRCRAFT, Vol. 47, No. 2*.

[4] Brezillon, J., Ronzheimer, A., Haar, D., et al. (2012). Development and application of multi-disciplinary optimization capabilities based on high-fidelity methods. In *53rd AIAA/ASME/ASCE/AHS/ASC Structures, Structural Dynamics and Materials Conference*.

[5] Grossman, B., Gurdal, Z., Strauch, G. J., et al. (1988). Integrated aerodynamic/structural design of a sailplane wing. *Journal of Aircraft, Vol 25, No.9*.

[6] Ghazlane, I., Carrier, G., and Dumont, A. (2012). Aerostructural adjoint method for flexible wing optimization. *AIAA Paper 2012-1924*.

[7] Kenway, G. K. W., Kennedy, G. J., and Martins, J. R. R. A. (2014). Scalable parallel approach for high-fidelity steady-state aeroelastic analysis and adjoint derivative computations. *AIAA Journal Vol. 52 No. 5*.

[8] Zhang, Z., Khosravi, S., and Zingg, D. W. (2017). High-fidelity aerostructural optimization with integrated geometry parameterization and mesh movement. *Struct. Multidisc. Optim. 55:1217-1235*.

[9] Marcelet, M., Peter, J., and Carrier, G. (2008). Sensitivity analysis of a strongly coupled system using the discrete direct and adjoint approach. *Revue Europenne de mcanique numrique*, 17, 1077–1106.

[10] Viti, A., Druot, T., and Dumont, A. (2016). Aero-structural approach coupled with direct operative cost optimization for new aircraft concept in preliminary design. In *17th AIAA/ISSMO Multidisciplinary Analysis and Optimization Conference, AIAA 2016-3512*.

[11] Blondeau, C., Achard, T., Girodroux-Lavigne, P., et al. (2015). Recent achievements towards aero-structure gradient computation using high-fidelity cfd-csm in the onera elsa software. In *International Forum on Aeroelasticity and Structural Dynamics, IFASD 2015, Saint Petersburg, Russia*.

[12] Girodroux-Lavigne, P. (2007). Recent navier-stokes aeroelastic simulations using the elsa code for aircraft applications. In *International Forum on Aeroelasticity and Structural Dynamics, Stockholm, Sweden*.

[13] Akgn, M. A., Haftka, R. T., Wu, K. C., et al. (2001). Efficient structural optimization for multiple load cases using adjoint sensitivities. *AIAA Journal Vol. 39 No.3*.

[14] Poon, N. M. K. and Martins, J. R. R. A. (2007). An adaptive approach to constraint aggregation using adjoint sensitivity analysis. *Structures and Multidisciplinary Optimization, Vol. 30, No. 1, pp. 61-73.*

[15] Achard, T., Blondeau, C., and Ohayon, R. (2016). An uncoupled approach to compute aero-structure gradients using high-fidelity cfd-csm. In *17th AIAA/ISSMO Multidisciplinary Analysis and Optimization Conference, AIAA AVIATION Forum, (AIAA 2016-4121)*.

[16] Achard, T., Blondeau, C., and Ohayon, R. (2017). High-fidelity aero-structure gradient computation techniques. application to the onera m6 wing. In *12th World Congress on Structural and Multidisciplinary Optimization*.

[17] Maute, K., Nikbay, M., and Farhat, C. (2001). Coupled analytical sensitivity analysis and optimization of three-dimensional nonlinear aeroelastic systems. *AIAA JOURNAL Vol. 39, No. 11*.

[18] Vanderplaats, G. N. and Salajegheh, E. (1989). New approximation method for stress constraints in structural synthesis. *AIAA Journal, Vol. 27, No. 3, pp. 352-358*.

[19] Vassberg, J. C., DeHann, M. A., Rivers, S. M., et al. (2008). Development of a common research model for applied cfd validation studies. *AIAA Paper 2008-6919*.

[20] Blondeau, C. and Salah El Din, I. (2012). A bi-level high fidelity aero-structural integrated design methodology - a focus on the structural sizing process. In *RAeS 3rd Aircraft Structural Design Conference, Delft, The Netherlands*.

[21] Vanderplaats, G. N. (1984). An efficient feasible directions algorithm for design synthesis. *AIAA Journal, Vol. 22, No. 11, pp. 1633-1640*.